Lamellar Phase of Stacked Two-Dimensional Rafts of Actin Filaments

Gerard C. L. Wong,[1,*] Alison Lin,[1] Jay X. Tang,[2] Youli Li,[1] Paul A. Janmey,[3] and Cyrus R. Safinya[1,†]

[1]*Materials Department, Physics Department, Biomolecular Science and Engineering Program, University of California, Santa Barbara, California 93106, USA*

[2]*Physics Department, Brown University, Providence, Rhode Island 02912, USA*

[3]*Institute for Medicine and Engineering, University of Pennsylvania, Philadelphia, Pennsylvania 19104, USA*

(Received 28 January 2003; published 2 July 2003)

We examined liquid crystalline phases of the cytoskeletal polyelectrolyte filamentous (F-)actin in the presence of multivalent counterions. As a function of increasing ion concentration, the F-actin rods in either an isotropic or a nematic phase will transform into a new and unexpected lamellar phase of cross-linked rafts (L_{XR} phase), before condensing into a bundled phase of parallel, close-packed rods. This behavior is generic for alkali earth divalent ions Mg^{2+}, Ca^{2+}, Sr^{2+}, and Ba^{2+}, and the structural transitions are achieved *without* any architecture-specific actin-binding linker proteins.

DOI: 10.1103/PhysRevLett.91.018103 PACS numbers: 87.16.Ka, 61.30.St, 61.30.Eb, 61.10.Eq

The most common starting point for understanding electrostatic interactions in aqueous media is screened Coulomb behavior, where like-charged objects, such as polyelectrolytes, charged globular proteins, or charged colloids, are expected to repel one another. These expectations are based on mean field theories, such as the Poisson-Boltzmann formalism and its variations, which are routinely employed in computational biology. In a landmark theoretical treatment [1], Oosawa first pointed out that fluctuations in the counterion charge density in the immediate vicinity of polyelectrolyte chains lead to long-range attractions which under certain conditions may overcome the electrostatic repulsion. Experimentally, it has been shown that like charged objects can, in fact, attract in the presence of multivalent ions [2], and this anomalous behavior has recently received intense theoretical scrutiny [3–8]. Although a complete consensus has not emerged, it is understood that counterions are important. The influence of counterions on the global symmetry of condensed polyelectrolyte phases and the structural evolution of these polyelectrolyte rod phases remains poorly understood.

In the present work, we considered F-actin as a model rodlike polyelectrolyte system, and examined its structural behavior in a wide range of divalent ions, using a combination of real-space and reciprocal-space methods to access structural information at length scales from microns to subnanometer. Filamentous actin (F-actin) is one of the principal components of eukaryotic cytoskeletons [2], and is essentially a helical rod (diameter $D_A \sim 80$ Å, persistence length $\xi_A \sim 10$ μm) with anionic linear charge density $\lambda_A \sim -e/2.5$ Å. We found that not only can attractive interactions exist between F-actin rods, but, as a function of increasing divalent ions, the global organization of F-actin rods can convert between different liquid crystalline phases consisting of distinct supramolecular assemblies with different symmetries and packing densities. In particular, we find an entirely new type of F-actin supramolecular structure in the presence of simple, divalent biological electrolytes such as Mg^{2+} and Ca^{2+}, which is distinct from the two well-known structures composed of close-packed bundles and cross-linked networks [9]. The basic unit of this new structure, shown in blue in Fig. 1, consists of two layers of F-actin rafts that are cross-linked via the electrolytes. The full three-dimensional structure consists of stacks of the two-layer rafts (Fig. 1, L_{XR}). The present results on ion linkers may have potential implications for cytoskeletal regulation, where F-actin is locally organized into bundles or networks for a wide range of intracellular functions in a

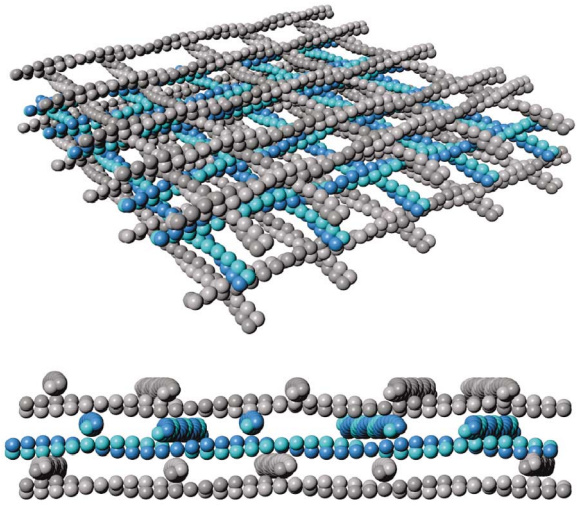

FIG. 1 (color). A schematic representation of the L_{XR} phase in which rafts of F-actin rods are cross-linked into a one-dimensional (1D) lamellar stack. Counterions (not shown for clarity), in the immediate vicinity of the rods due to Manning condensation, are localized to the crossing regions between actin rods. One of the cross-linked bilayer rafts (i.e., a 3D unit cell) has been highlighted in blue for clarity. The graph on the bottom depicts a side view of the structure shown on the top.

 0031-9007/03/91(1)/018103(4)$20.00

highly coordinated process, which is thought to be achieved using protein linkers exclusively at present.

The progressive condensation of F-actin with increasing multivalent ion concentration can be seen even at optical length scales. Figure 2(a) shows the optical images of F-actin solution samples (2 mg/ml, average length ~1000 Å, controlled using gelsolin, an actin severing and capping protein) at three different Ca^{2+} concentrations (top to bottom: 2.5, 9.0, and 80 mM. Sample preparation details are described elsewhere [10]). Condensates of different character can be observed in the 9.0 mM and the 80 mM samples. The 9.0 mM sample has condensed into a translucent phase, while the 80 mM sample has condensed into a dense, essentially opaque phase. Figures 2(b)–2(d) are the same three samples observed under crossed polarizers. The 2.5 mM uncondensed sample is an isotropic phase, with no observable birefringence [Fig. 2(b)]. In contrast, the strong observed birefringence signals for the 9.0 mM [Fig. 2(c)] and 80 mM [Fig. 2(d)] samples clearly demonstrate their liquid crystalline nature. The existence of a new intermediate condensed phase [Figs. 2(a) middle and 2(c)] is quite unexpected, as it is usually assumed that in the presence of simple divalent counterions there are only two states, where the rods form either a dilute, uncondensed phase [Figs. 2(a) top and 2(b)] or a condensed bundled phase [Figs. 2(a) bottom and 2(d)] [2].

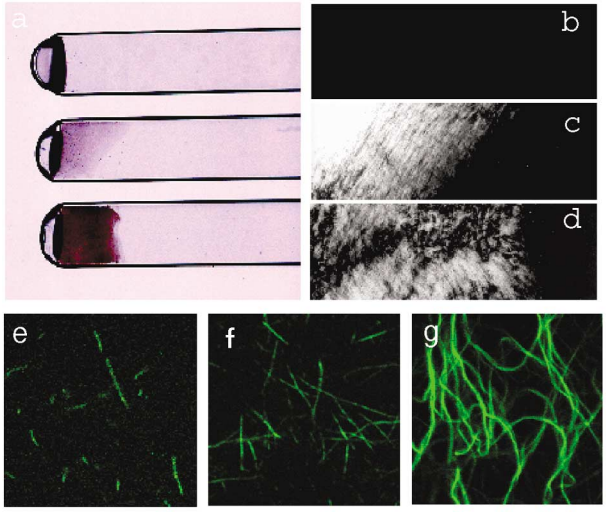

FIG. 2 (color). (a) Condensation of F-actin filaments (2 mg/ml, average length ~100 nm) with $CaCl_2$. The $CaCl_2$ concentrations are 2.5, 9.0, and 80 mM for the top, middle, and bottom capillaries, respectively. The 2D nematic LC network phase exists in the middle capillary, where a phase boundary can be observed. The distinct bundled phase can be seen in the bottom capillary for contrast. These samples are stable for months. (b),(c),(d) Polarized micrographs taken from the top, middle, and bottom capillaries, respectively. Note the strong birefringence in both the network phase and the bundled phase. The bottom panel shows laser scanning confocal microscope images of a dilute solution (0.03 mg/ml) of ~10 μm F-actin filaments at (e) 2.5, (f) 9, and (g) 80 mM $CaCl_2$. The field of view is 25 μm × 25 μm. Although the global concentration of F-actin is constant, the ion-induced condensation transitions have progressively increased the local concentrations in (e)–(g). In (f), the system is dominated by nonparallel filament cross-links, while in (g), the filaments have condensed into a parallel arrangement and have formed an ensemble of thick bundles. Note the dramatically increased fluorescence intensity from the multifilament bundles.

To investigate the behavior of individual filaments in real space, we examined dilute solutions of F-actin at different multivalent ion concentrations using confocal fluorescence microscopy [Figs. 2(e)–2(g)]. Even though excluded volume interactions, which drive liquid crystalline ordering in the more concentrated solutions, are essentially absent in these dilute solutions, the propensity for network formation, which is necessary for the L_{XR} phase, can already be observed [8]. It can be seen [Fig. 2(e)] that a dilute (0.03 mg/ml) solution of F-actin (~ 10 μm average length) at 0.2 mM Ca^{2+} (contained in the actin buffer) is in an uncondensed isotropic phase. At 9 mM Ca^{2+} [Fig. 2(f)], however, a sample at the same global concentration is dominated by pointlike filament intersections. In contrast, as the Ca^{2+} concentration is further increased to 80 mM, F-actin filaments condense into thick parallel bundles [Fig. 2(g)]. It would be interesting to see if a similar raft phase occurs for filamin-linked F-actin at high concentrations [11].

To investigate the molecular organization of these condensed phases, a series of high-resolution synchrotron small-angle x-ray scattering (SAXS) measurements were performed on F-actin solutions (average length ~1000 Å) in the presence of four divalent counterions (Ca^{2+}, Mg^{2+}, Sr^{2+}, Ba^{2+}) primarily in the concentration range between 3 and 80 mM (for x-ray sample preparation and experimental details see [10]). A sequence of condensed phases is formed as the divalent ion concentration is increased. Because the x-ray data characteristic of each phase is similar for the four counterions, we show here only SAXS data for one (Ca^{2+}) system. The SAXS data for the new intermediate phase (3.0 mM Ca^{2+}) unambiguously demonstrates that it is a new form of liquid crystalline matter [Fig. 3(a)]. The 2D diffraction pattern is composed of two sets of correlation peaks along different directions. This indicates that both the continuous translational and rotational symmetries of the isotropic phase have been broken. The first set of these peaks, as shown on the horizontal section of the diffraction pattern [Fig. 3(b)] along axis 1, is composed of three sharp peaks that index exactly to a quasi-Bragg reflection at $q_1 = 0.033$ Å^{-1} ($d = 190$ Å) and its higher harmonics $q_n = nq_1$. These peaks are the diffraction signature of a 1D layered structure. The layer spacing is slightly larger than twice the F-actin hard core diameter, and corresponds well to the periodicity expected from a 1D lamellar stack of raftlike bilayer sheets of F-actin cross-linked

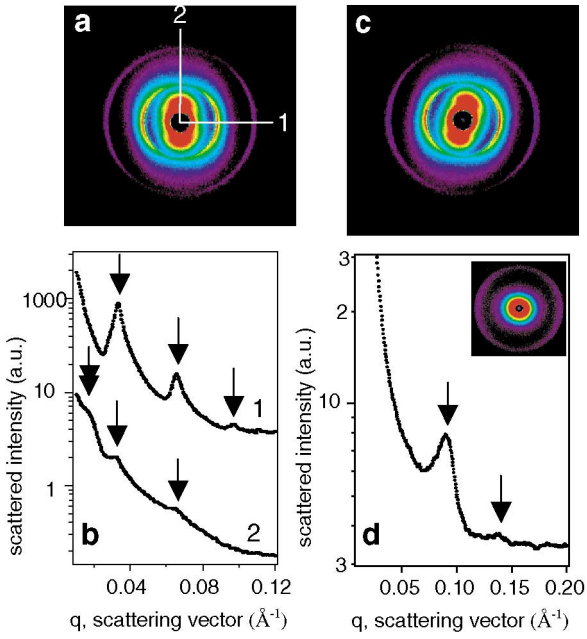

FIG. 3 (color). (a) Two-dimensional (2D) SAXS data of a partially aligned condensed L_{XR} phase composed of 100 nm F-actin condensed by 3.0 mM $CaCl_2$. (b) Top: a cut of the diffraction pattern in (a) along axis 1, showing three strong harmonics of the layering peaks. Bottom: a cut of the diffraction pattern along axis 2, showing a distinct set of broad correlation peaks. The weak liquidlike, short-ranged correlation peak marked by the double-headed arrow corresponds to a nematic arrangement of F-actin at a direction orthogonal to that of the layering direction. Weak intensity from the lamellar peaks can still be detected (single arrows), due to the large mosaic distribution. (c) SAXS data from the same sample in (a) but on a different spot. A number of domains with different orientation can be seen as a 300 μm $\times$ 300 μm synchrotron x-ray beam is scanned across the sample. This indicates that the L_{XR} phase has a multiaxial structure, and does not have a single preferred orientation. (d) Inset: 2D SAXS pattern from a partially aligned sample in the bundled phase, with 100 nm F-actin condensed by 80 mM $CaCl_2$. The plot shows radially averaged SAXS data showing the close-packed inter-rod correlation characteristic of the bundled phase.

by divalent ions. No other arrangement of F-actin will allow a close enough interfilament distance for an attractive interaction. A schematic representation of this lamellar L_{XR} phase is shown in Fig. 1. The actin rods are arranged parallel to the layers with the axial direction of F-actin perpendicular to the layer normal direction. This arrangement is qualitatively different from all known lamellar or smectic arrangements of rodlike molecules. In addition to the lamellar peaks, a distinct set of broad correlation peaks, which appear along the axis labeled 2 in Figs. 3(a) and 3(b) (two headed arrow), is now visible at $q = 0.016$ Å^{-1}. These weak liquidlike, short-ranged correlations correspond to a nematic arrangement of F-actin within a raft at a direction orthogonal to that of the layering direction, with an average inter-rod distance of 393 Å. It is interesting to note that the measured surface-to-surface distance between actin in adjacent layers ($\sim$ 15 Å) is too large to accommodate a typical salt bridge. Moreover, it must be stressed that no cross correlations between adjacent layers of actin rods, which are expected from crystalline samples, are observed.

The x-ray patterns on occasion showed partial orientation of the L_{XR} phase within the size of the synchrotron beam (300 μm $\times$ 300 μm). Indeed, we observe variations in the orientation of the 2D SAXS pattern within the same capillary sample holder as the x-ray beam illuminates different regions [compare Figs. 3(a) and 3(c)]. This indicates that this new bulk 3D layered phase is oriented on the scale of the x-ray beam with the layer normal meandering with the sample on the millimeter scale. Moreover, in the SAXS patterns for a small fraction of samples ($< 3\%$), the short-range correlations along axis 2 are not perpendicular to the quasi-long-range-layering order along axis 1 [see, for example, Fig. 3(c)]. We interpret this as diffraction contributions from multiple domains, although a higher order biaxiality in the organization of the rods within the layers may also be possible.

In order to produce the observed lamellar peaks with a layer spacing $\approx$ 2 times the diameter of F-actin, neighboring F-actin sheets must be crossed at some angle with respect to each other, as we show schematically in Fig. 1. Furthermore, the concentration of F-actin within each sheet must be different to produce the required electron density variations between neighboring sheets leading to the observed SAXS peak. We note that such a unit cell structure of crossed sheets of F-actin is consistent with expectations from electrostatics where repulsion between like-charged rods is maximal for parallel rods and minimal for 90° crossed rods [4,12]. Indeed, it is likely that in this intermediate concentration range, where the condensed counterion concentration is not sufficient to fully neutralize F-actin, the divalent ions help stabilize this structure by cross-linking F-actin rods at large angles to each other to minimize the electrostatic repulsion between parallel rods in adjacent layers. In addition to electrostatics, a number of other effects in rodlike systems are also likely to be relevant to the formation of the L_{XR} phase [8,13], structural relatives of which may have been observed using specific protein linkers [14].

As the ion concentration is increased, the L_{XR} phase collapses into uniaxial bundles. The behavior is indicated by the SAXS pattern in Fig. 3(d), inset, in which 100 nm F-actin rods are condensed by 80 mM of Ca^{2+}. The SAXS data clearly indicate the formation of bundles, and the first diffraction peak at $1 = 0.089$ Å^{-1} [Fig. 3(d)] corresponds well to the diameter of F-actin, and implies a close-packing of actin rods within the bundle. The packing of F-actin rods within these bundles exhibit short-range order, with domain sizes of the same order

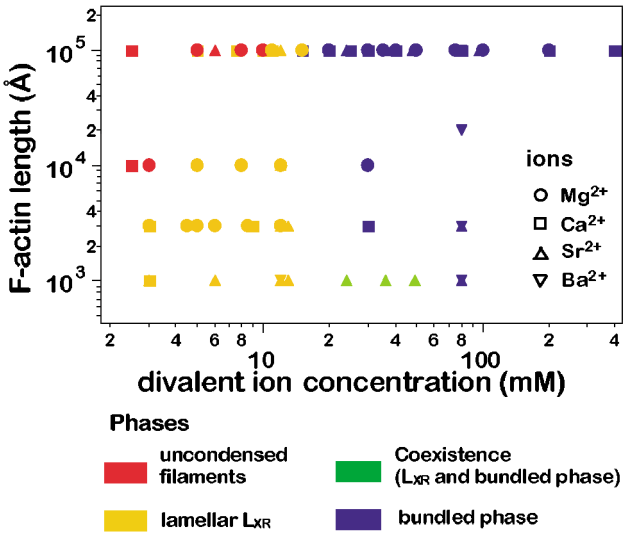

FIG. 4 (color). A phase diagram for four different divalent ions from the alkali earth column (Mg^{2+}, Ca^{2+}, Sr^{2+}, Ba^{2+}, represented by different symbols), in which the phase behavior as a function of divalent ion concentrations and rod length is summarized. For example, the onset of ion-induced condensation of actin into the L_{XR} lamellar raft phase with Mg^{2+} for 3000 Å actin filaments occurs at Mg^{2+} concentrations as low as 3 mM, and increases to 5 mM for 1 μm actin and 11 mM for 10 μm actin filaments. Furthermore, although the phase boundaries shift slightly for different ions, it can be seen that the basic phase behavior is general for all four ion species: As the divalent ion concentration is increased, the system evolves from an uncondensed isotropic phase to the condensed L_{XR} raft phase, and finally to the condensed bundled phase.

as the diameter of actin. A weak higher order reflection can also be observed at $q = 0.139$ Å^{-1}. This value deviates slightly from the position expected from an exact hexagonal arrangement of rods. The SAXS from this bundle phase of F-actin is clearly distinct from that of the L_{XR} 3D stacks of rafts.

The observed phase behavior is generic for a wide range of different divalent ions. Figure 4 is a phase diagram for four different divalent ions (Mg^{2+}, Ca^{2+}, Sr^{2+}, Ba^{2+}), in which the phase behavior as a function of divalent ion concentrations and rod length is summarized. For short F-actin rods, the L_{XR} phase exists over a wide ($>$ 50 mM) range of divalent concentrations. As the average length of the F-actin rods is increased (and becomes increasingly nematic), this strong layering behavior is substantially weaker for 10 μm long F-actin. The L_{XR} phase exists only over a narrow ($\sim$ 5 mM) range of divalent concentrations for such filaments, and the associated correlation peaks become less intense. More importantly, these phases may be relevant at physiological ionic strengths. For example, total Mg levels within the cell can be as high as 10 mM, and much of it is actually incorporated into various cellular structures [15]. The orange filled circles in the phase diagram denote the Mg^{2+}-induced L_{XR} phase. It can be seen that only 3 mM Mg^{2+} is required to condense 3000 Å actin filaments into the L_{XR} raft phase, with progressively higher critical concentrations for longer filaments: 5 mM and 11 mM Mg^{2+} for 1 and 10 μm filaments, respectively.

In summary, we have found a new lamellar phase of F-actin rafts cross-linked by divalent ions and shown that the supramolecular linking architecture of F-actin can be controlled without using any actin linking proteins, by using nonspecific ion linkers alone.

We are especially grateful to R. Bruinsma for numerous extensive and insightful discussions. We thank Nate Bouxsein and Thomas E. Angelini for help with the SAXS data on Mg^{2+}. This work was supported by NIH GM-59288, NSF-DMR-0203755, CTS-0103516, and DMR-0080034 to UCSB; NSF-DMR-0071761, DOE DEF-G02-91ER45439, and Cystic Fibrosis Foundation (CFF) WONG01I0 to UIUC; NIH HL-67286 and CFF No. 00G0 to University of Pennsylvania; and NSF-DMR-0071761 to Brown University.

*Corresponding author.
Email address: gclwong@uiuc.edu
Present address: Department of Material Science and Engineering, Department of Physics, Department of Bioengineering, University of Illinois, Urbana-Champaign, IL 61801, USA.
†Corresponding author.
Email address: safinya@mrl.uscb.edu

[1] F. Oosawa, *Polyelectrolytes* (Marcel Dekker, New York, 1971); Biopolymers **6**, 1633 (1968).
[2] J. X. Tang and P. A. Janmey, J. Biol. Chem. **271**, 8556 (1996).
[3] N. Gronbech-Jensen *et al.*, Phys. Rev. Lett. **78**, 2477 (1997).
[4] B. Y. Ha and A. J. Liu, Phys. Rev. Lett. **79**, 1289 (1997); **81**, 1011 (1998).
[5] A. P. Lyubartsev *et al.*, Phys. Rev. Lett. **81**, 5465 (1998).
[6] M. J. Stevens, Phys. Rev. Lett. **82**, 101 (1999); B. I. Shklovskii, Phys. Rev. Lett. **82**, 3268 (1999).
[7] I. Borukhov, R. Bruinsma, W. M. Gelbart, and A. J. Liu, Phys. Rev. Lett. **86**, 2182 (2001).
[8] I. Borukhov and R. Bruinsma, Phys. Rev. Lett. **87**, 158101 (2001).
[9] H. Lodish *et al.*, *Molecular Cell Biology* (Freeman, New York, 2000), 4th ed.
[10] G. C. L. Wong *et al.*, Science **288**, 2035 (2000).
[11] L. Limozin and E. Sackmann, Phys. Rev. Lett. **89**, 168103 (2002).
[12] V. A. Parsegian, J. Chem. Phys. **56**, 4393 (1972).
[13] A. Stroobants *et al.*, Phys. Rev. Lett. **57**, 1452 (1986); X. Wen and R. B. Meyer, Phys. Rev. Lett. **59**, 1325 (1987).
[14] L. Hou, K. Luby-Phelps, and F. Lanni, J. Cell Biol. **110**, 1645 (1990).
[15] See, for example, A. Romani, C. Marfella, and A. Scarpa, Miner. Electrolyte Metabol. **19**, 282 (1993).